Journal of Sound and Vibration (2000) **238**(2), 271–293
doi:10.1006/jsvi.2000.3102, available online at http://www.idealibrary.com on IDEAL®

ESTIMATION OF VIBRATION DISTRIBUTION FOR FINITE STRUCTURES

J. LIANG AND B. A. T. PETERSSON

Department of Aeronautical and Automotive Engineering, Loughborough University, Loughborough LE 11 3*TU, England*

(*Received* 4 *December* 1999, *and in final form* 12 *May* 2000)

The distribution of vibration over finite structures excited by a force is considered. To describe the vibration distribution, a quantity, called motion transmissibility, is introduced which is defined as the ratio of the velocity of the structure at an arbitrary point to that at the excitation location. This quantity can be of substantial assistance to achieve reduction in the modelling of built-up structures. It is found that for rods, beams and shells, the motion transmissibility can be estimated by using the corresponding semi-infinite structure. For plates, the motion transmissibility can be estimated by considering the corresponding quarter-infinite structure.

1. INTRODUCTION

With a view towards the development of a simple method for estimating the vibration of built-up structures, the information required for primary and secondary substructures has been studied. Thereby, primary and secondary structures refer to substructures which strongly and weakly influence the dynamic behaviour of the assembly respectively. It is noticed [1] that if the structure is composed of substructures between which dynamic mismatch exists, the establishment of the system description revealing the salient physics requires different dynamic characteristics for the different classes of substructures. For some substructures mobility is required, while for others, the vibration distribution, normalized by the vibration at the excitation point, is necessary. Herein such a normalized vibration distribution is termed *motion transmissibility* and a notation T_{qp} is used,

$$T_{qp}(\omega) = v_q(\omega)/v_p(\omega) \quad \text{or} \quad T_{qp}(\omega) = Y_{qp}(\omega)/Y_{pp}(\omega) \tag{1}$$

where ω is angular frequency, v_q and v_p are the velocities at an arbitrary point q and the excitation point p respectively. Y_{qp} is the transfer mobility from point p to q, and Y_{pp} the point mobility (a list of symbols can be found in Appendix C).

From linear system theory the transfer function of a system, represented here by the mobility, is characterized by both poles and zeros (see, for example, reference [2]), whereas from the definition equation (1) the motion transmissibility by the zeros only. It should, therefore, be possible to estimate motion transmissibility by using only a part of the structural detail or alternatively from a reduced model of the structure. A test of this idea on rods reveals that the motion transmissibility can indeed be exactly determined from the vibration of the corresponding semi-infinite rod. Therefore, once this has been demonstrated to be the case also for other systems, such as beams, plates and shells, the analysis of the built-up structures under consideration can be facilitated by employing

0022-460X/00/470271 + 23 $35.00/0

markedly reduced and simplified models for those substructures where information of vibration distribution suffice for the description of the dynamic behaviour of a built-up system.

2. ONE-DIMENSIONAL SYSTEMS

2.1. RODS

The motion of rods under axial excitation belongs to the class of one-dimensional wave motion. With a force excitation at $x = x_p$, (see Figure 1), the velocity of the rod, upon assuming free–free boundary conditions, is given by [3]

$$v(x) = \frac{Y_c F}{\mathrm{j}\sin(kL)} \begin{cases} \cos k(L - x_p)\cos(kx) & \text{for } x < x_p \\ \cos kx_p \cos k(L - x) & \text{for } x \geqslant x_p, \end{cases} \tag{2}$$

where Y_c is the characteristic mobility of the rod, and $k = \omega\sqrt{\rho/E}$ is the wavenumber. Accordingly, the motion transmissibility of the rod is found to be

$$T_{qp} = \frac{v_q}{v_p} = \begin{cases} \cos kx_q / \cos kx_p & \text{for } x_q < x_p, \\ \cos k(L - x_q)/\cos k(L - x_p) & \text{for } x_q \geqslant x_p. \end{cases} \tag{3}$$

If two semi-infinite rods are considered, one being infinite in the positive x direction with its free end at $x = 0$ and the other in the negative x direction with its free end at $x = L$, as shown in Figures 2(a) and 2(b) respectively. The velocity of the semi-infinite rod in case (a) is expressed by the sum of the direct wave and the reflection from the left end as

$$v^{(a)}(x) = \tfrac{1}{2} Y_c F(\mathrm{e}^{-\mathrm{j}k|x - x_p|} + \mathrm{e}^{-\mathrm{j}k(x + x_p)}) = Y_c F \begin{cases} \mathrm{e}^{-\mathrm{j}kx_p}\cos kx & \text{for } x \leqslant x_p, \\ \mathrm{e}^{-\mathrm{j}kx}\cos kx_p & \text{for } x \geqslant x_p \end{cases} \tag{4}$$

and that in case (b) as

$$v^{(b)}(x) = \tfrac{1}{2} Y_c F(\mathrm{e}^{-\mathrm{j}k|x - x_p|} + \mathrm{e}^{-\mathrm{j}k(2L - x - x_p)}) = Y_c F \begin{cases} \mathrm{e}^{jk(x - L)}\cos k(x_p - L) & \text{for } x \leqslant x_p, \\ \mathrm{e}^{jk(x_p - L)}\cos k(x - L) & \text{for } x \geqslant x_p. \end{cases} \tag{5}$$

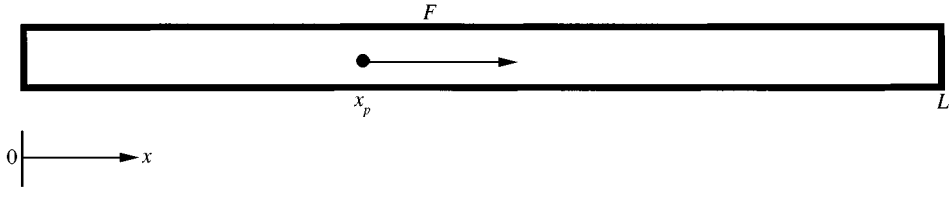

Figure 1. A rod excited by a force.

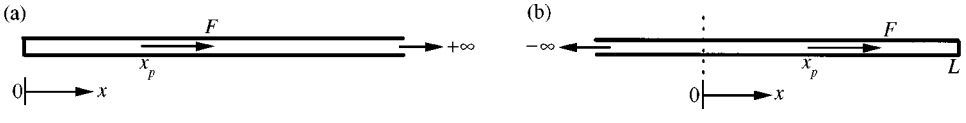

Figure 2. Two semi-infinite rods: (a) infinite in the positive x direction; (b) infinite in the negative x direction.

From equations (4) and (5), the motion transmissibilities for the two semi-infinite rods are obtained as

$$T_{qp}^{(a)} = \begin{cases} \cos kx_q / \cos kx_p & \text{for } x_q \leqslant x_p, \\ 1 & \text{for } x_q \geqslant x_p \end{cases}, \tag{6}$$

and

$$T_{qp}^{(b)} = \begin{cases} 1 & \text{for } x_q \leqslant x_p, \\ \cos k(x_q - L)/\cos k(x_p - L) & \text{for } x_q \geqslant \mathrm{x}_p. \end{cases} \tag{7}$$

Upon comparing $T_{qp}^{(a)}$, $T_{qp}^{(b)}$ with T_{qp} it is observed that

$$T_{qp} = \begin{cases} T_{qp}^{(a)} & \text{for } x_q \leqslant x_p, \\ T_{qp}^{(b)} & \text{for } x_q > x_p, \end{cases} \tag{8}$$

which states that the motion transmissibility of finite, elementary one-dimensional systems can be calculated from the corresponding semi-infinite system. Thereby, the term elementary is used to distinguish the present system from such which support both propagating and evanescent waves, such as beams.

It should be noted that although equation (8) is derived for free–free boundary conditions, it is, by means of the image source method [4, 5], readily demonstrated to hold also for any other boundary condition.

The reason why $T_{qp}^{(a)}$ and $T_{qp}^{(b)}$ are applicable in different regions is found by considering the standing and travelling wave fields. With the excitation applied at x_p, the direct wave propagates to left in the region $x < x_p$ and to right in the region $x > x_p$. The direct wave, combined with the reflection from the left end, forms a standing wave field in the region $x < x_p$ whereas a travelling wave is obtained in the region $x > x_p$. Thus, $T_{qp}^{(a)}$ is not applicable for the case where $x_q > x_p$, and $T_{qp}^{(b)}$ is not applicable for the case where $x_q < x_p$.

2.2. BEAMS IN FLEXURE

Beams differ from the elementary one-dimensional system in which near fields can arise at the excitation and the two ends. Even if, as in the situation with simple supports at the boundaries, the near fields vanish in the vicinity of the ends, that at the excitation generally remains. This may introduce a complication in estimating the motion transmissibility from the corresponding semi-infinite structure as suggested in section 2.1 and the applicability of such an estimation must therefore be investigated.

Figure 3(a) illustrates the constituent waves for the vibration of a finite beam, transversely excited by a force at x_p. For positions where $x_q < x_p$, the motion transmissibility of the

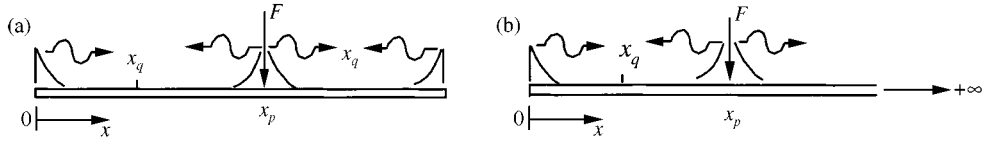

Figure 3. Illustration of the near and travelling wave fields in beams.

finite length beam is to be compared with that of the corresponding semi-infinite beam, infinite in positive x direction, as shown in Figure 3(b). Where $x_q > x_p$, the comparison should be made with the corresponding semi-infinite beam extending in the negative x direction instead.

For a harmonic excitation, two different types of direct waves are generated; the direct travelling wave v_f^∞ and the direct evanescent wave v_n^∞. As v_f^∞ impinges on the two ends, four reflections generally result, two travelling and two evanescent reflections. These four reflections are then repeatedly reflected, resulting in an infinite sequence of reflections. The total field which is initially associated with v_f^∞ can be denoted by v^{I}. Similarly, as v_n^∞ impinges on the two ends, four reflections result, two travelling and two evanescent reflections. Again, these four reflections are repeatedly reflected at the ends, resulting in another infinite set of reflections. A notation v^{II} may be used to denote the field which stems from v_n^∞. By the superposition principle, the total wave field v in the beam is given by

$$v = v^{\mathrm{I}} + v^{\mathrm{II}}. \tag{9}$$

In many applications, the beam considered vibrates in a frequency range above its first few eigenfrequencies. This occurs when the beam is several times longer than the wavelength, making the evanescent wave from one end negligibly small as it reaches the opposite end. Hence, those multiple reflections due to the evanescent part from each end can be neglected. A further simplification can be obtained by restricting the location of the excitation to be more than half a wavelength away from both ends, making those reflections associated with v_n^∞ negligible and v^{II} being approximated by $v^{\mathrm{II}} \approx v_n^\infty$, rendering only a small contribution to the total wave field, and thus, v^{II} can be neglected. With these considerations, the expression for v can be simplified as (see the wave approach for beams in reference [4])

$$v = C_{ff}^L(v_f^\infty + v_{ff}^L + v_{nf}^L), \quad x < x_p, \tag{10}$$

where v_{ff}^L, v_{nf}^L are the left-hand travelling and evanescent reflections due to v_f^∞ incidence, respectively, and C_{ff}^L is given by

$$C_{ff}^L = \frac{1 + r_{ff}^R \mathrm{e}^{-\mathrm{j}2k(L-x_p)}}{1 - r_{ff}^L r_{ff}^R \mathrm{e}^{-\mathrm{j}2kL}}. \tag{11}$$

Herein, r_{ff}^L, r_{ff}^R are the reflection coefficients of the left and right ends respectively. By the same token, the wave field of the corresponding semi-infinite beam of infinite extent in the positive x direction can be written as

$$v^{semi} = v_f^\infty + v_{ff}^L + v_{nf}^L. \tag{12}$$

Upon comparing equations (12) and (10) it is seen that

$$v = C_{ff}^L v^{semi}, \tag{13}$$

and accordingly

$$T_{qp} = v_q/v_p = T_{qp}^{semi}, \quad x_q < x_p. \tag{14}$$

In the same manner, the relation for positions where $x_q > x_p$ can be obtained from the comparison of the finite beam with the corresponding beam of infinite extent in negative x direction. Accordingly, it can be concluded that if the beam is more than a wavelength long and the excitation point is at least half a wavelength away from each end, the motion transmissibility of the finite length beam can be estimated from the corresponding semi-infinite beam.

For the case where the excitation point is within half a wavelength of any of the ends, the wave field associated with the direct evanescent wave cannot be neglected. Owing to the difficulty of analytically describing such a case, a numerical approach will be used in section 5 for the detailed investigation.

3. TWO-DIMENSIONAL SYSTEMS

Obviously, it would be useful if the method of estimating the motion transmissibility for one-dimensional systems also were applicable in two-dimensional cases. In this pursuit a simply supported plate, excited by a point force F, is considered; see Figure 4. Other, inhomogeneous boundary conditions will be investigated numerically in section 5.

The transverse displacement of such a plate can be expressed by a series expansion [6] as

$$(x, y, k) = \frac{F}{4DA} \sum_{m=-\infty}^{\infty} \sum_{n=-\infty}^{\infty} \frac{1}{(k_{x,m}^2 + k_{y,n}^2)^2 - k^4} \{ e^{-j(k_{m,x}(x_p - x) + k_{y,n}(y_p - y))} - e^{-j(k_{m,x}(x_p + x) + jk_{y,n}(y_p - y))} - e^{-j(k_{m,x}(x_p - x) + k_{y,n}(y_p + y))} + e^{-j(k_{m,x}(x_p + x) + k_{y,n}(y_p + y))} \} \quad (15)$$

where $k_{x,m} = m\pi/L_x$, $k_{y,n} = n\pi/L_y$ and k is the flexural wavenumber of the plate. D is the bending stiffness of the plate and $A = L_x L_y$ is the area of the plate. It is noted that in equation (15), the indices m and n run from $-\infty$ to $+\infty$, see also reference [3].

To evaluate the displacement w in the region $x \leqslant x_p$, $y \leqslant y_p$, two approximations are introduced. First, the whole frequency range is divided into a number of narrow bands at a span equal to the modal overlap $\Delta\omega$. For the lth band, the modes inside are grouped with the use of an approximation $k_{mn} \approx k_l$, k_l being the mean of k_{mn} in that band. Second, it is assumed that the number of modes in each band is sufficiently large so that the mode grouping can be approximately evaluated by an integral. This means that the double series sum in equation (15) is reduced to a single sum over k_l, $l = 1, 2, 3, \ldots$. The major effect of

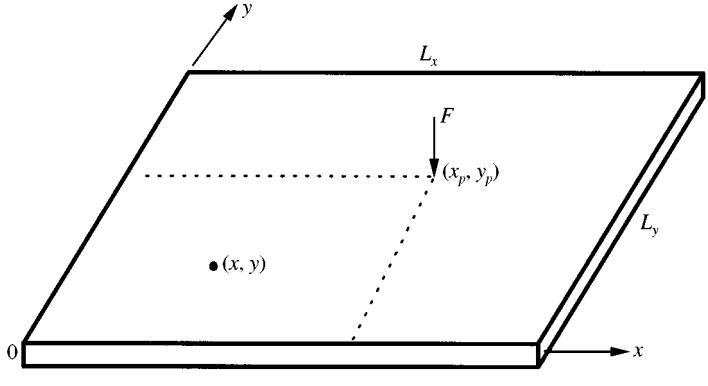

Figure 4. A rectangular plate excited by a point force at (x_p, y_p).

employing the two approximations is that the representation of the dynamic characteristics of the plate in the frequency domain is numerically smoothed. For the situation where the two approximations are appropriate, this "smoothing effect" is restricted locally and the global characteristics will remain unaffected.

Upon evaluating the single-series sum, by using a contour integral [7–9], the displacement of the plate is approximately obtained as (see details in Appendices A and B)

$$w(x, y, k) \approx -\frac{F}{2\pi Dk^2 \tan(k\pi/\Delta \mathrm{k})}(S_0 + S_1 + S_2 + S_3) \quad \text{for } \leqslant x_p,\ y \leqslant y_p, \tag{16}$$

where

$$S_0 = +[\mathrm{H}_0^{(2)}(kr_0) - \mathrm{H}_0^{(2)}(-\mathrm{j}kr_0)], \qquad S_1 = -[\mathrm{H}_0^{(2)}(kr_1) - \mathrm{H}_0^{(2)}(-\mathrm{j}kr_1)],$$

$$S_2 = -[\mathrm{H}_0^{(2)}(kr_2) - \mathrm{H}_0^{(2)}(-\mathrm{j}kr_2)] \qquad S_3 = +[\mathrm{H}_0^{(2)}(kr_3) - \mathrm{H}_0^{(2)}(-\mathrm{j}kr_3)], \tag{17}$$

see also reference [10]. Therefore, the motion transmissibility of the plate is obtained from

$$T_{qp} = \frac{w(x_q, y_q, k)}{w(x_p, y_p, k)} \approx \frac{(S_0 + S_1 + S_2 + S_3)_{(x_q, y_q)}}{(S_0 + S_1 + S_2 + S_3)_{(x_p, y_p)}} \quad \text{for } x_q \leqslant x_p, y_p, y_q \leqslant y_p. \tag{18}$$

In equation (17), S_0 is the direct wave radiated from the source. S_1, S_2, S_3 can be interpreted as the waves radiated from the three image sources located at $(-x_p, y_p)$, $(x_p, -y_p)$ and $(-x_p, -y_p)$ respectively [3, 11]. It is realized that the wave field represented by the sum $(S_0 + S_1 + S_2 + S_3)$ is the same as that in the corresponding quarter-infinite plate extending to infinity in positive x and y directions; see Figure 5. Hence, equation (18) suggests that the motion transmissibility of the simply supported plate can be estimated from its corresponding quarter-infinite plate.

It should be noted that the above result can easily be extended to arbitrary response points on the plate. For a given excitation position, the plate can be divided into four areas, as shown in Figure 6.

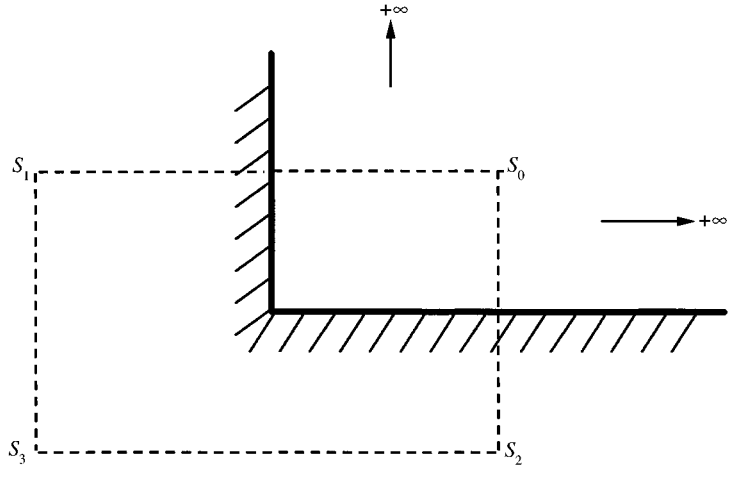

Figure 5. Quarter-infinite plate and its three image sources.

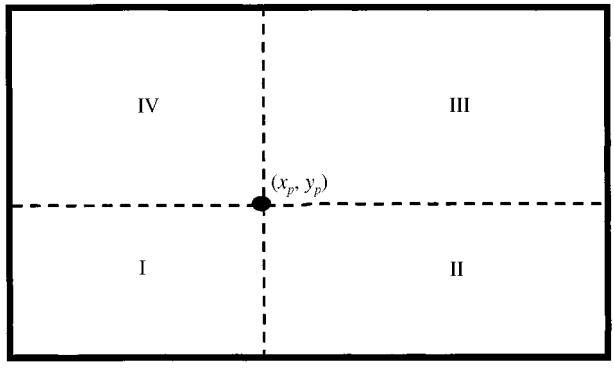

Figure 6. Subdivision of the plate in four quadrants with respect to excitation position.

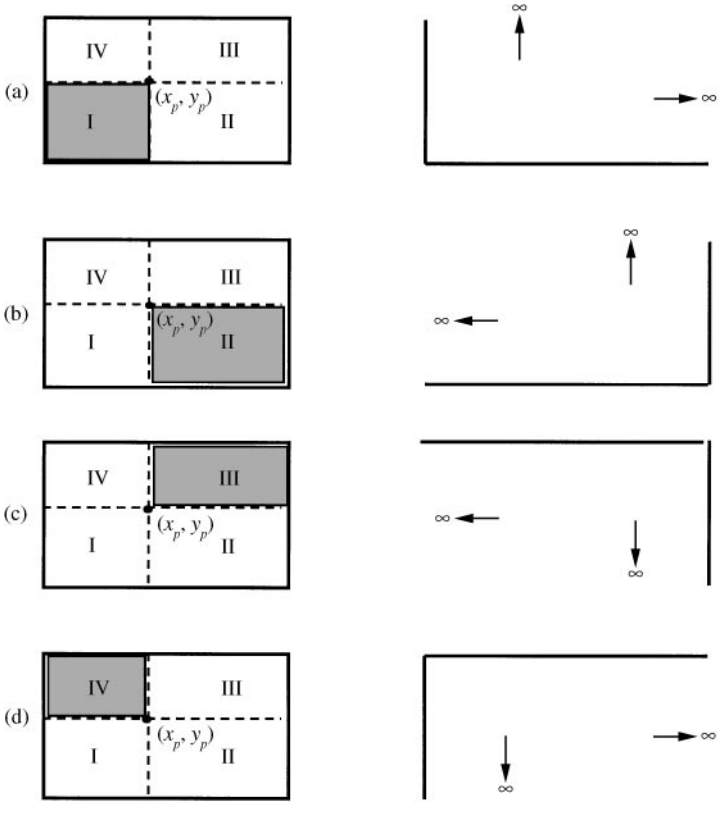

Figure 7. Choice of the corresponding quarter-infinite plate according to the location of response point (x_q, y_q).

If the response point q is located in area I, then the appropriate corresponding quarter-infinite plate is obtained by displacing the upper and right edges to infinity, see Figure 7(a). With the response point q in area II, the left and upper edges are displaced, etc. Figures 7(b), 7(c) and 7(d) show the situations where the response points are in the areas II, III and IV respectively.

Owing to the two approximations involved, the applicability of the method described above will be subject to conditions. As is well known, the first approximation is appropriate for the situation where the ratio of the modal overlap to the central frequency of the small band is much less than unity, i.e., $\Delta\omega/\omega = \eta \ll 1$. This condition can be generally satisfied for ordinary material properties and if the plate is not submerged in a dense medium. The second approximation is obviously appropriate when, in agreement with, for example, reference [3], the modal overlap $\Delta\omega$ is much larger than the average of the frequency interval between modes $\delta\omega$.

4. SHELLS

The shell motion involves three components, longitudinal, torsional and flexural. With respect to the zero order circumferential mode, $n = 0$(breathing mode), only the first two components are involved whereas a higher order circumferential mode, $n \geqslant 1$, is associated with all three.

When the shell is subject to uniform axial or circumferential excitation only, the breathing mode dominates the motion so that the shell behaves like either a rod or a shaft. Hence, the motion transmissibility can be estimated by using the corresponding semi-infinite shell according to the study of elementary one-dimensional systems.

In the absence of the axial and circumferential excitation, however, the breathing mode can be ignored [4] and the transverse displacement of the shell is predominant and can be expressed by a series expansion [12–14]

$$w(x, \theta) = \sum_{\mathrm{n}=1}^{\infty} W_{\mathrm{n}}(x)\cos n\theta, \tag{19}$$

where

$$W_n(x) = \sum_{q=1}^{4} (C_{q,n}^{+}\mathrm{e}^{-\mathrm{j}k_{q,n}x} + C_{q,n}^{-}\mathrm{e}^{\mathrm{j}k_{q,n}(x-L)}). \tag{20}$$

The wavenumbers $k_{q,n}$, $q = 1, 2, 3, 4$, represent four different wavenumbers for nth circumferential mode and, $C_{q,n}^{\pm}$, $q = 1, 2, 3, 4$ are constant coefficients which are determined by the boundary conditions. By following Flügge's shell theory [13], the real and imaginary parts of the wavenumbers are plotted versus frequency in Figures 8 for a group of circumferential modes. From these graphs, the following observations can be made.

Well below the ring frequency ω_{ring}, $k_{1,n}$, $k_{2,n}$, $k_{3,n}$and $k_{4,n}$ are all complex, indicating that all waves in the shell decay exponentially with distance. Especially, the large imaginary parts of $k_{1,n}$ and $k_{2,n}$ ($k_{1,n}^{(I)}R \approx k_{2,n}^{(I)}R \approx 5$ approximately) suggest that the $k_{1,n}$ and $k_{2,n}$ waves diminish quickly and can be neglected. Furthermore, it is seen from Figures 8(c) and 8(d) that the imaginary parts of $k_{3,n}$ and $k_{4,n}$ increase rapidly with order of the circumferential mode n, suggesting that the associated waves can also be neglected for higher order, $n \geqslant 2$. Hence, below ω_{ring}, the motion of the shell is dominated by $k_{3,n=1}$ and $k_{4,n=1}$ waves. Moreover, Figure 8(c) shows that below ω_{ring} the $k_{3,n=1}$ wave is not a propagating wave but evanescent. With the argument employed in conjunction with beams, the $k_{3,n=1}$ wave can be neglected for not too short cylinders. Accordingly the transverse displacement of the shell can be approximated in terms of the $k_{4,n=1}$ wave as

$$w(x, \theta) \approx A(\theta)\mathrm{e}^{-\mathrm{j}k_{4,n=1}^{(R)}x} + B(\theta)\mathrm{e}^{+\mathrm{j}k_{4,n=1}^{(R)}(x-L)} \quad \text{for } \omega < \omega_{ring}. \tag{21}$$

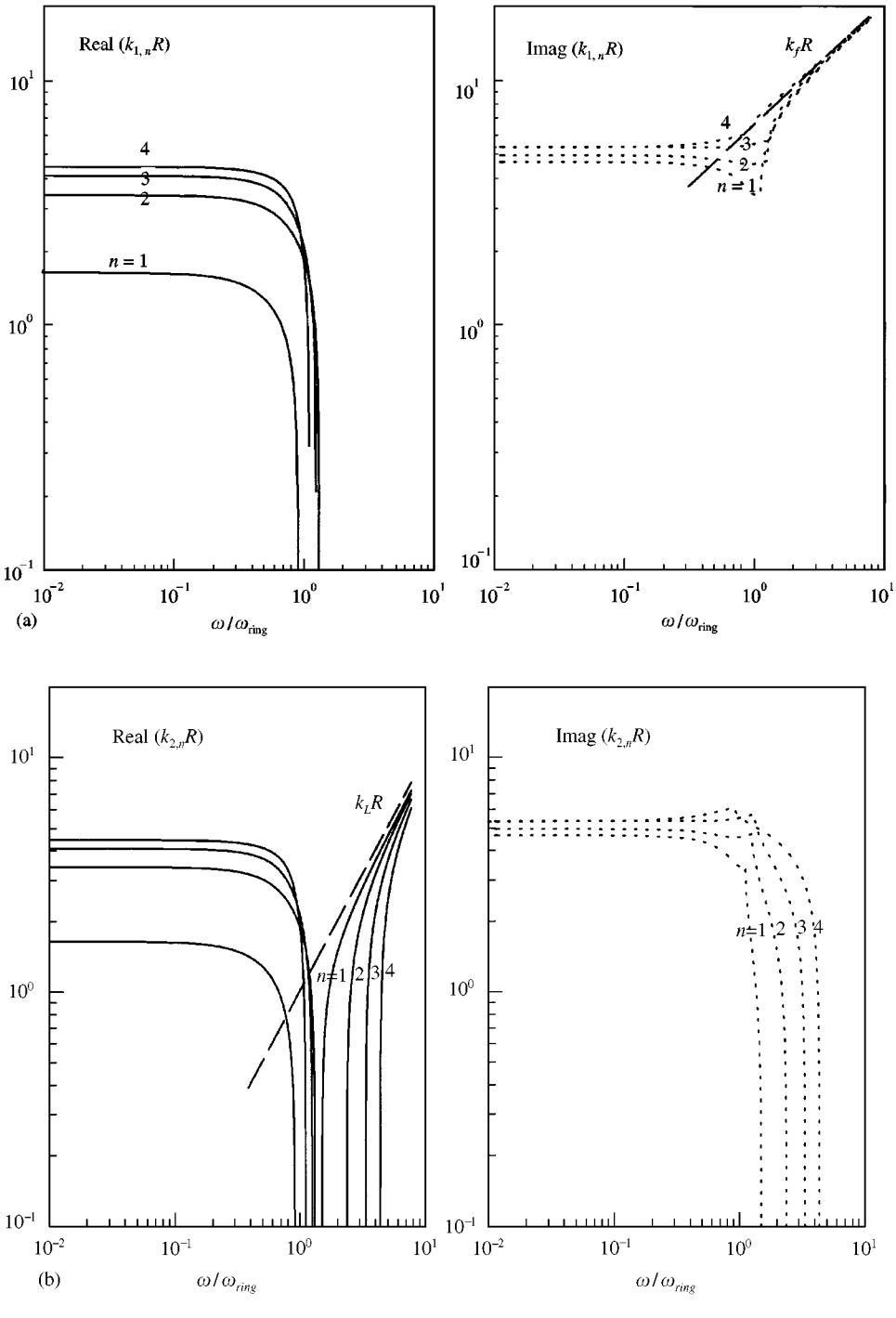

Figure 8. Non-dimensional wavenumber versus non-dimensional frequency ω/ω_{ring}: (a) $k_{1,n}R$; (b) $k_{2,n}R$; (c) $k_{3,n}R$; (d) $k_{4,n}R$.

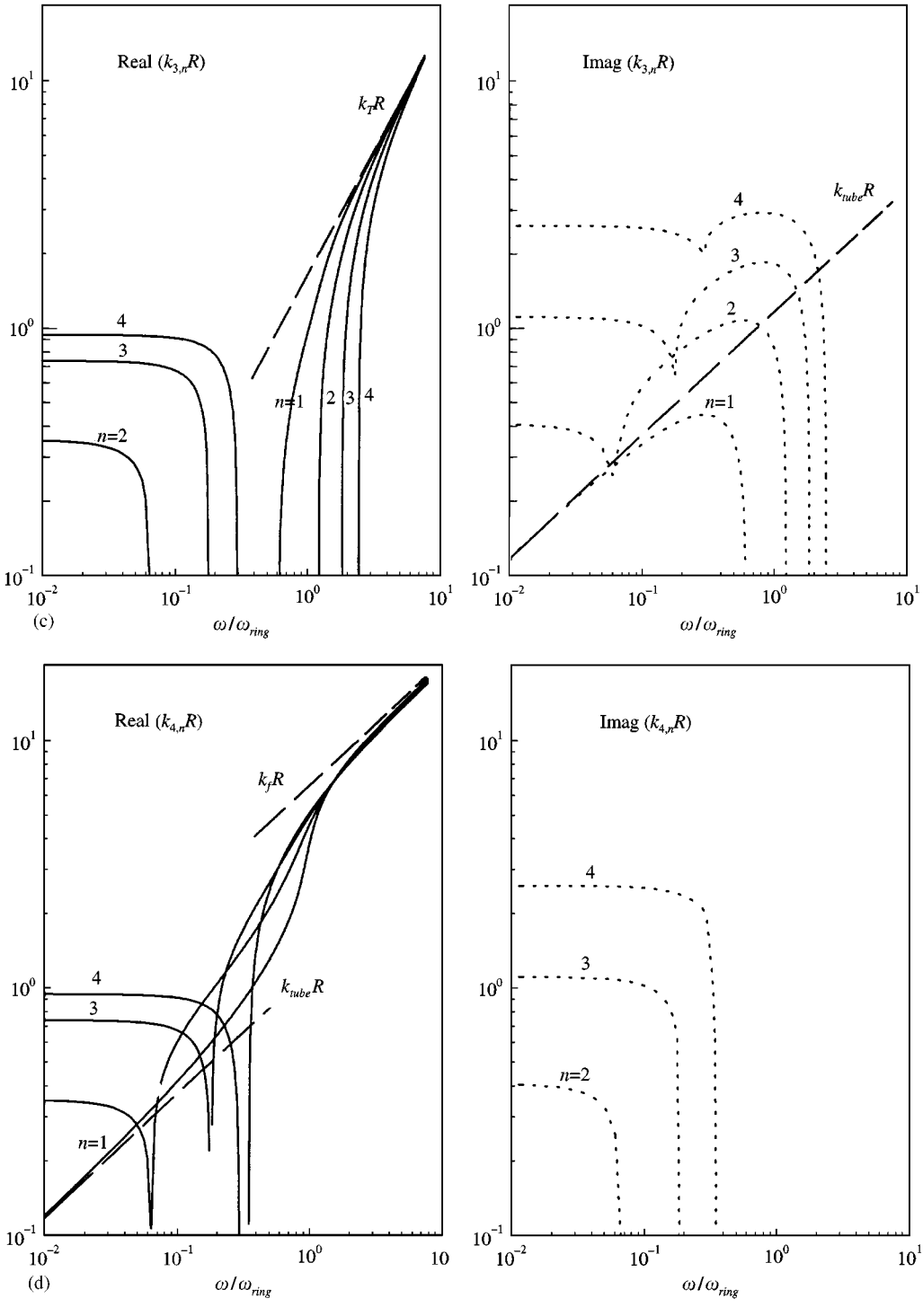

Figure 8. Continued.

Since equation (21) is of the same kind as that of the elementary one-dimensional system with respect to the axial variable x, it follows from the result for rods that, below ω_{ring}, it is applicable to estimate the motion transmissibility of the shell using the corresponding semi-infinite shell.

Far above ω_{ring}, it is seen that $k_{1,n}$ is purely imaginary, representing an evanescent wave, whereas $k_{2,n}$, $k_{3,n}$ and $k_{4,n}$ are purely real, representing three propagating waves. Furthermore, it is seen that the real parts of $k_{2,n}$ and $k_{3,n}$ tend to k_L and k_T—the wavenumbers of longitudinal and torsional waves, respectively, and the real part of $k_{4,n}$ tends to k_f—the wavenumber of a plate having a thickness equal to the wall thickness of the shell. In the absence of axial and circumferential excitations, $k_{2,n}$ and $k_{3,n}$ waves will be insignificant and can be neglected. Thus, the transverse displacement of the shell is approximately written in the form

$$w(x, \theta) \approx A(\theta)\mathrm{e}^{-\mathrm{j}k_f x} + B(\theta)\mathrm{e}^{+\mathrm{j}k_f(x-L)} \quad \text{for } \omega > \omega_{ring}. \tag{22}$$

Again, the form of equation (22) is identical to that of a rod with respect to an axial variable x such that the conclusion drawn for rods will apply and above ω_{ring} the motion transmissibility of the shell can be estimated by using the corresponding semi-infinite shell.

Near ω_{ring}, it is seen that both the real and imaginary parts of $k_{1,n}$, $k_{2,n}$, $k_{3,n}$ and $k_{4,n}$ exhibit steep drops in magnitude at different frequencies, implying that all wave types must be taken into account. Owing to the difficulty in examining this region analytically, a numerical investigation was conducted and is described in the next section.

5. COMPUTATIONAL INVESTIGATION

5.1. BEAMS

The motion transmissibility for a free–free steel beam (length: 1 m, width: 6 mm, thickness: 50 mm) has been calculated to corroborate the applicability of estimating the motion transmissibility of beams by considering the corresponding semi-infinite beam in the presence of near fields. The calculation is based on Euler–Bernoulli beam theory [4]. The beam is subjected to force excitation at one end. This makes the two near fields in the vicinity of the excitation and the end coincident, achieving maximum contribution from the evanescent waves to the field. In the calculation, the loss factor is taken to be $\eta = 0{\cdot}003$. In Figure 9 are shown the estimated motion transmissibilities T^{esti} together with the complete one $T^{complete}$. Above $kL = 1$, it is seen that T^{esti} matches the tendency and major variation of $T^{complete}$ with Helmholtz number, including the case that the response point is located at the other end of the beam. The major differences observed are in peak and trough amplitudes. Below $kL = 1$, T^{esti} is seen to be invalid. The calculation was also carried out for the same beam but for an increased loss factor of $\eta = 0.04$. The results are presented in Figure 10. At this level of damping, it is seen that the peak and trough differences in the range above $kL = 1$ are greatly reduced. Therefore, the method appears applicable for Helmholtz numbers above unity and improves as the damping increases.

5.2. PLATES

A simply supported square steel plate (side length: 2 m, thickness 2 mm) is considered to corroborate the method for two-dimensional systems and to establish limits of applicability.

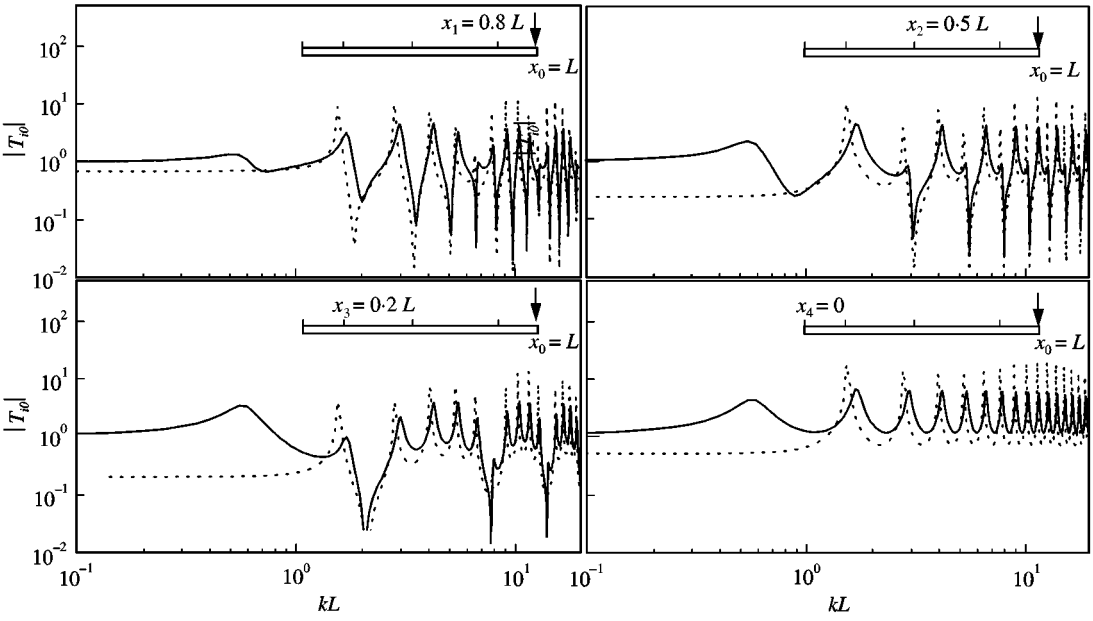

Figure 9. Motion transmissibility of a free–free beam, $\eta = 0{\cdot}003$: (——), T^{esti}; (· · · · · ·), $T^{complete}$.

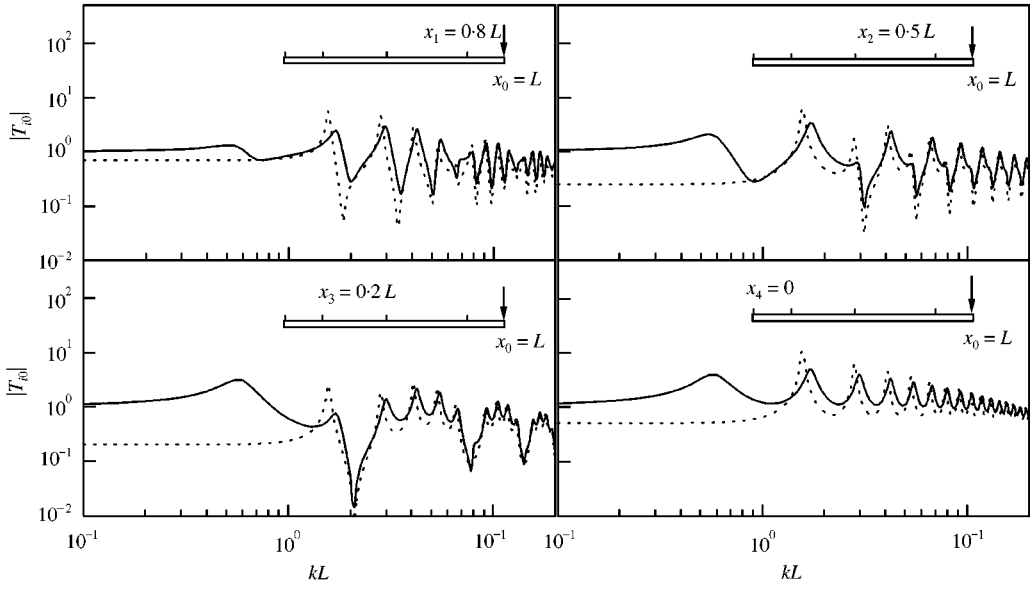

Figure 10. Motion transmissibility of a free–free beam, $\eta = 0{\cdot}04$: (——), T^{esti}; (· · · · · ·), $T^{complete}$.

Plotted in Figure 11 is the estimated motion transmissibility T^{esti} as well as the complete one $T^{complete}$, calculated from a modal expansion with 3600 modes ($m, n = 1,2,\ldots,60$), used to ensure stable convergence. In the calculation, the loss factor is taken to be $\eta = 0{\cdot}08$ to ensure that the condition $\Delta\omega \gg \delta\omega$ is satisfied over a wide frequency range. Position 0 in the

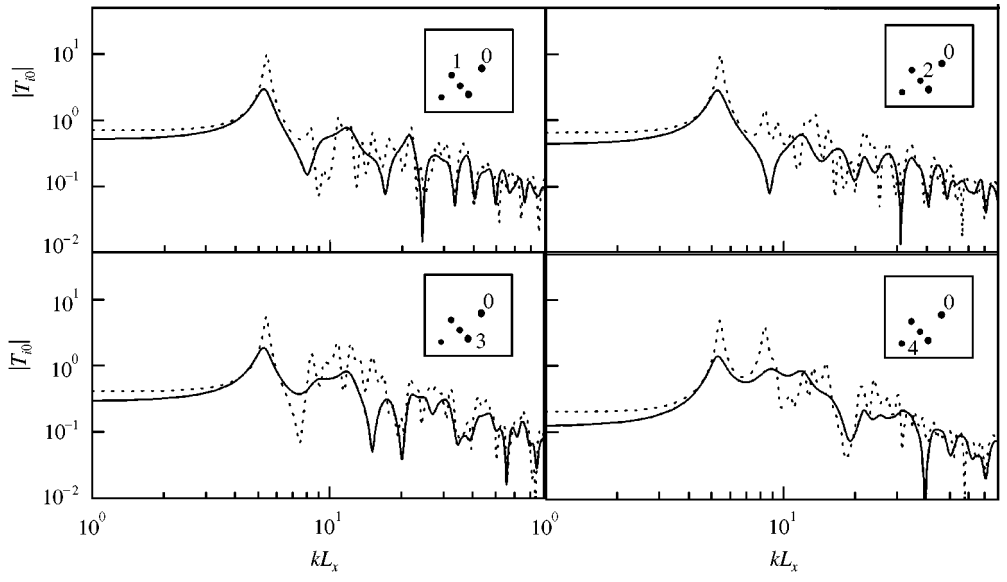

Figure 11. Motion transmissibility of a simply supported plate, $\eta = 0{\cdot}08$: (·····), T^{esti}; (·····), $T^{complete}$.

graph is that of the excitation. For $kL_x \geqslant 1$, it is seen that T^{esti} reveals the trend and captures the major variation with Helmholtz number. The major difference is again found in peak and trough magnitudes. When $kL_x < 1$, the T^{esti} is inapplicable.

In order to clarify whether the above estimation method is applicable also for inhomogenous boundary conditions, the motion transmissibility of the same plate was re-calculated for free–free boundary conditions, where $T^{complete}$ is calculated from a modal expansion including 334 modes. Lemke's results summarized in reference [6] are used for the six lowest eigenfrequencies and eigenfunctions. The higher order modes are found by using Warburton's formula [15]. T^{esti} is obtained from that of a simply supported quarter-infinite plate plus a correction term which accounts for free boundary conditions [16]. It is seen from the graph in Figure 12 that also for these boundary conditions T^{esti} reveals the trend and captures the major variation with Helmholtz number, including the cases where the response point is near an edge or in a corner.

To examine the influence of damping on the applicability of T^{esti}, the motion transmissibility was calculated for four different loss factors, $\eta = 0{\cdot}003$, $0{\cdot}012$, $0{\cdot}04$, $0{\cdot}08$, under simply supported boundary conditions. The results are compiled in Figure 13. For a small loss factor, $\eta = 0{\cdot}003$, it is seen that T^{esti} fails to give a useful estimation. As η is increased, the difference between T^{esti} and $T^{complete}$ decreases and with a loss factor, $\eta = 0{\cdot}04$, T^{esti} can give a reasonable estimation. Since $\Delta\omega = \eta\omega$, the results thus highlight the necessity to satisfy the criterion $\Delta\omega \gg \delta\omega$.

In the investigation so far, the effect of the aspect ratio of the plate has not been taken into account. For rectangular plates, $k_{x,m}$ has a different interval than $k_{y,n}$. Consequently, the mode grouping in the ring-shaped wavenumber bands is performed over different ranges of x and y mode indices. This difference is ignored in the integral approximation. To examine its influence, the simply supported plate is given four different aspect ratios. In the calculations, the area and thickness of the plate are held constant. This is necessary to retain the same modal density in all cases. The loss factor is again taken to be $\eta = 0{\cdot}08$ to satisfy the modal overlap condition over a wide range. The excitation is applied at $x_0 = 0{\cdot}75L_x$,

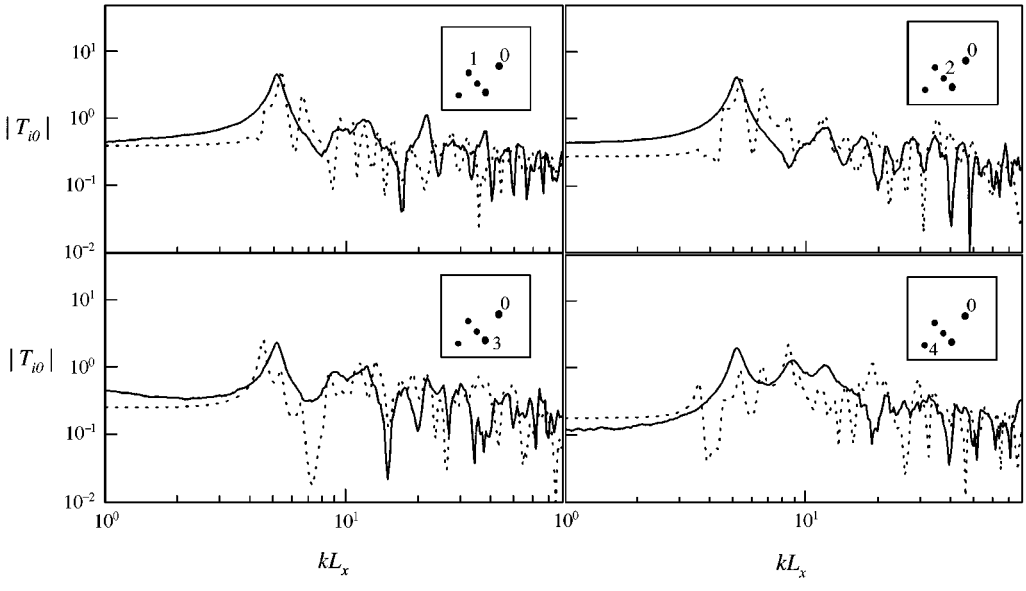

Figure 12. Motion transmissibility of a free–free plate, $\eta = 0{\cdot}08$: (——), T^{esti}; (·····), $T^{complete}$.

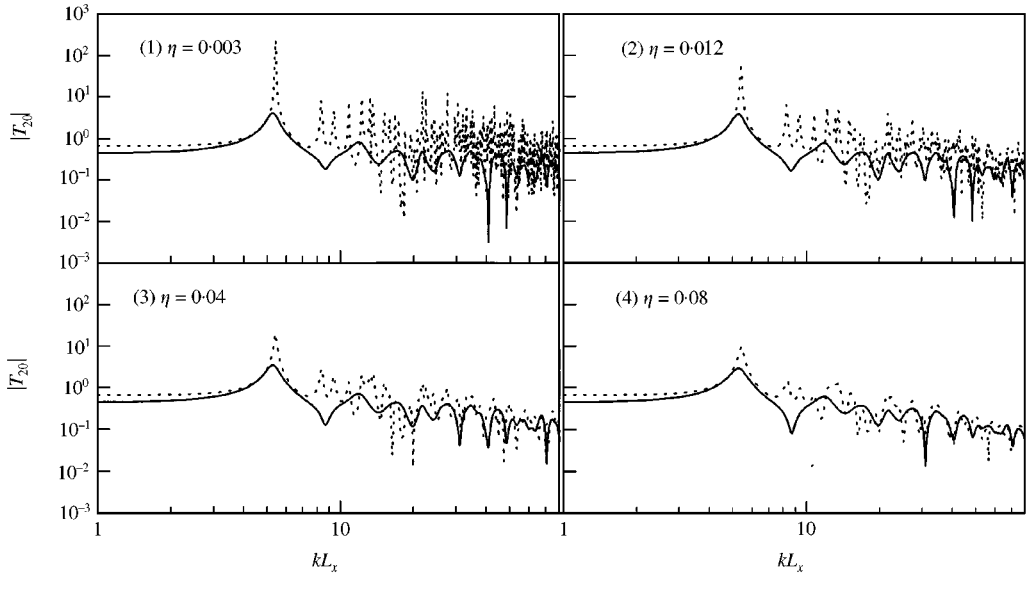

Figure 13. Motion transmissibility of a plate for four different loss factors: (·····), T^{esti}; (·····), $T^{complete}$.

$y_0 = 0{\cdot}6L_y$, and the response point is located at $x_1 = 0{\cdot}3L_x$, $y_1 = 0{\cdot}2L_y$. The results are plotted in Figure 14 versus kL_c, where $L_c = \sqrt{L_x L_y}$ is the characteristic dimension of the plate. Below $L_y/L_x = 0{\cdot}7$, it is seen that the influence of the aspect ratio is marked, whereas above it is negligible. It seems, therefore, appropriate to state that the method is most suitable for nearly square plates.

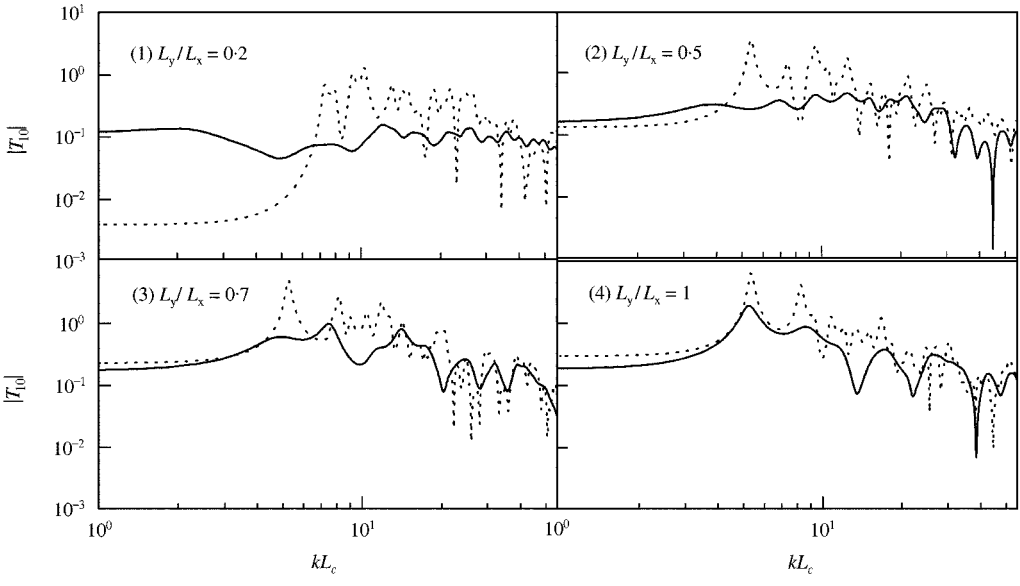

Figure 14. Influence of the aspect ratio of plate: (——), T^{esti}; (·····), $T^{complete}$.

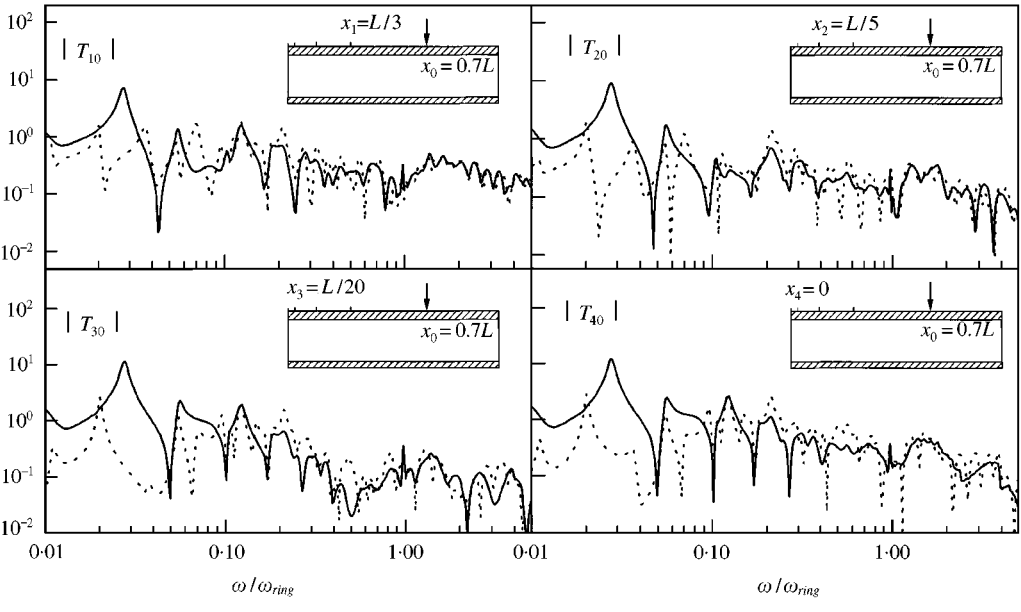

Figure 15. Motion transmissibility of a shell, $\theta = 0$: (——), T^{esti}; (·····), $T^{complete}$.

5.3. CYLINDRICAL SHELLS

To test the method for estimating the motion transmissibility with respect to shells, a free–free cylindrical shell is considered. Shown in Figure 15 and 16 are the plots of estimated motion transmissibility T^{esti} established from the corresponding semi-infinite shell and the complete one $T^{complete}$, calculated by using a wave approach [4, 17] and

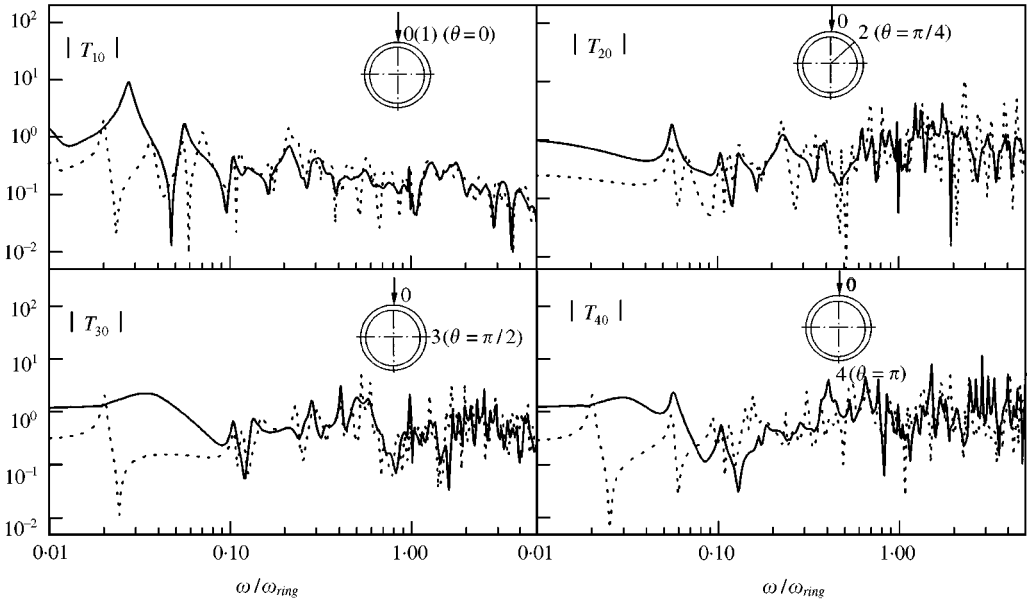

Figure 16. Motion transmissibility of a shell for different circumferential angle θ: (——), T^{esti}; (·····), $T^{complete}$.

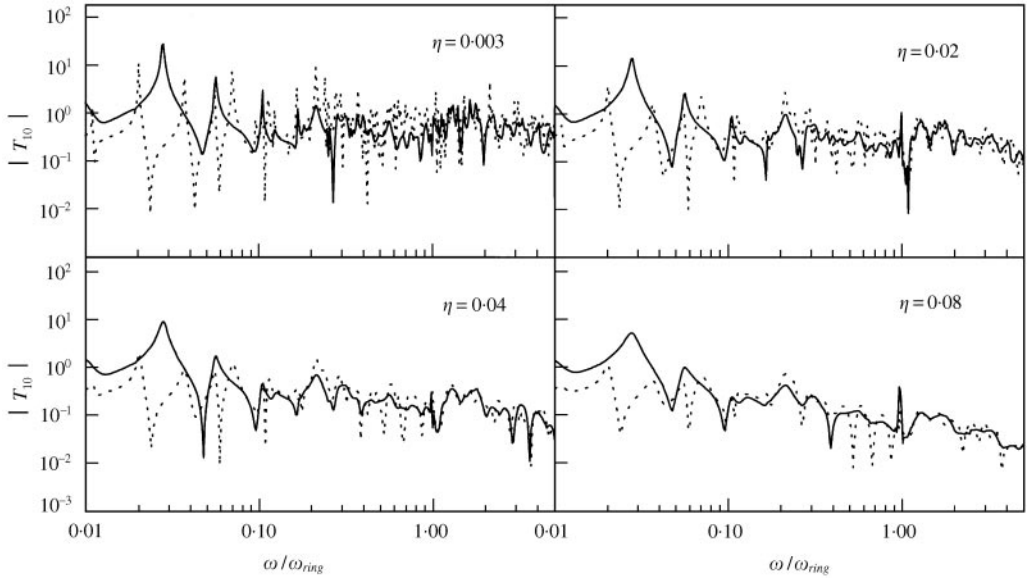

Figure 17. Influence of damping: (——), by semi-infinite shell; (·····), by finitelength shell.

assuming Flügges shell theory [13]. The results are displayed versus non-dimensional frequency ω/ω_{ring}, where ω_{ring} is the ring frequency of the shell. In the calculations, a loss factor of $\eta = 0{\cdot}04$ is assumed. Figure 15 depicts a case where the axial position for the response is varied for a fixed circumferential angle of $\theta = 0$, whereas Figure 16 refers to a varied circumferential angle θ for a fixed axial position. Above $\omega/\omega_{ring} = 0{\cdot}05$, it is seen that T^{esti} produces meaningful results with respect to tendency and captures the major

variation with frequency, including the region near ring frequency. Below $\omega/\omega_{ring} = 0{\cdot}05$, T^{esti} deviates markedly from the complete solution.

The motion transmissibility of the shell was also re-calculated for other loss factors and the results are displayed in Figure 17. With small losses, i.e., $\eta = 0{\cdot}003$, it is seen that the discrepancy between T^{esti} and $T^{complete}$ is large. For $\eta = 0{\cdot}02$, T^{esti} begins to give a reasonable estimation. In accordance with what was found for beams, this thus demonstrate that the method works better for large losses.

6. CONCLUDING REMARKS

In the preceding sections, a method has been investigated by which the distribution of vibration over generic structures is evaluated in an overall sense from models employing the associated semi- or quarter-infinite structures. Thereby, a semi-infinite structure is used when one-dimensional systems are considered while a quarter-infinite structure is substituted for two-dimensional ones such that primary wave reflections are taken into account.

The method is rigorously proven for elementary, one-dimensional systems such as rods, or shafts and to be applicable for beams where near fields explain the difference in peak and trough magnitudes between the estimated and the complete motion transmissibilities. For plates, the method can give valid estimations in the range where the modal overlap bandwidth is much greater than the average interval between the eigen-frequencies. It is also demonstrated that the method is applicable for damped cylindrical shells in a range above $\omega/\omega_{ring} = 0{\cdot}05$.

REFERENCES

1. J. LIANG 1999 *Ph.D. Thesis, Loughborough University*, U.K. Analysis of dominating dynamic characteristics of structures.
2. D. E. NEWLAND 1989 *Mechanical Vibration Analysis and Computation*. London: Longman Group UK Limited.
3. E. SKUDRZYK 1980 *The Journal of Acoustical Society of America* **67**, 1105–1135. The mean-value method of predicting the dynamic response of complex vibrators.
4. L. CREMER, M. HECKL and E. E. UNGAR 1988 *Structure-borne Sound*. Berlin: Springer, second edition.
5. A. D. PIERCE 1981 *Acoustics: An Introduction to its Physical Principles and Applications*. New York: McGraw-Hill.
6. A. W. LEISSA 1993 *Vibration of Plates*. Acoustical Society of America (Originally issued by NASA, 1973).
7. M. G. JUNGER and D. FEIT 1986 *Sound, Structures, and their Interaction*. Cambridge, MA: The MIT press, second edition.
8. P. M. MORSE and H. FESHBACH 1953 *Methods of Theoretical Physics, Vol.* 1. New York: McGraw-Hill Book Company.
9. S. HANISH 1981 *A treatise on Acoustics Radiation*. Washington, D.C., U.S.A.: Naval Research Laboratory, second edition.
10. B. A. T. PETERSSON 1993 *Journal of Sound and Vibration* **160**, 67–91. Structural acoustic power transmission by point moment and force excitation; Part 2: plate-like structures.
11. R. GUNDA and S. M. VIJAYKAR and R. SINGH 1995 *Journal of Sound and Vibration* **185**, 791–808. Methods of images for the harmonic response of beams and rectangular plates.
12. A. W. LEISSA 1993 *Vibration of Shells*. Acoustical Society of America (Originally issued by NASA, 1973).
13. M. FLÜGGE 1967 *Stresses in Shell*. Berlin: Springer-Verlag, fourth printing.
14. M. HECKL 1962 *Journal of the Acoustical Society of America* **34**, 1553–1557. Vibrations of point-driven cylindrical shells.

15. G. B. WARBURTON, 1954 *Proceedings of the Instiute of Mechanical Engineers* **168**, 371–384. The vibration of rectangular plates.
16. R. GUNDA, S. M. VIJAYKAR, R. SINGH and J. E. FARSTAD 1998 *Journal of the Acoustical Society of America* **103**, 888–899. Harmonic Green's function of a semi-infinite plate with clamped or free edges.
17. D. J. MEAD 1991 *Journal of Sound and Vibration* **144**, 507–530. The response of infinite periodic beams to point harmonic force: a flexural wave analysis.
18. M. ABRAMOWITZ and I. A. STEGUN 1965 *Handbook of Mathematical Functions*. New York: Dover.

APPENDIX A: AN APPROXIMATE EXPRESSION FOR THE TRANSVERSE DISPLACEMENT OF PLATES EXCITED BY A CONCENTRATED FORCE

Consider the mode series expansion of the transverse displacement of simply supported plates as given in equation (15). If the response point (x, y) is confined to the region $x \leqslant x_p$, $y \leqslant y_p$ and the abbreviations

$$\begin{aligned} k_{mn} &= \sqrt{k_{x,m}^2 + k_{y,n}^2}, \quad \theta_{mn} = \tan^{-1}(k_{y,n}/k_{x,m}), \\ r_0 &= \sqrt{(x_p - x)^2 + (y_p - y)^2}, \quad \alpha_0 = \sin^{-1}\{(y_p - y)/r_0\}, \\ r_1 &= \sqrt{(x_p + x)^2 + (y_p - y)^2}, \quad \alpha_1 = \sin^{-1}\{(y_p - y)/r_1\}, \\ r_2 &= \sqrt{(x_p - x)^2 + (y_p + y)^2}, \quad \alpha_2 = \sin^{-1}\{(y_p + y)/r_2\}, \\ r_3 &= \sqrt{(x_p + x)^2 + (y_p + y)^2}, \quad \alpha_3 = \sin^{-1}\{(y_p + y)/r_3\}, \end{aligned} \tag{A1}$$

are introduced where the distances r_i and angles α_i, $i = 0, 1, 2, 3$ are illustrated geometrically in Figure A.1, then equation (15) can be rewritten as

$$\begin{aligned} w(x, y, k) = \frac{F}{4DA} \sum_{k_{mn}=0}^{\infty} \frac{1}{k_{mn}^4 - k^4} \sum_{0 \leqslant \theta_{mn} \leqslant 2\pi} \{ & e^{-j k_{mn} r_0 \cos(\theta_{mn} - \alpha_0)} - e^{-j k_{mn} r_1 \cos(\theta_{mn} - \alpha_1)} \\ & - e^{-j k_{mn} r_2 \cos(\theta_{mn} - \alpha_2)} + e^{-j k_{mn} r_3 \cos(\theta_{mn} - \alpha_3)} \}. \end{aligned} \tag{A2}$$

Following the approach outlined in section 3 and with reference to the graph of the mode lattice of the plate in Figure A2, the mode grouping for each concentric ring-shaped band Δk, which corresponds to a narrow frequency band as described in section 3, is approximately given by

$$\begin{aligned} w_{\Delta k}(k_l) \approx \frac{F}{4DA} \frac{1}{k_l^4 - k^4} \sum_{0 \leqslant \theta_{mn} \leqslant 2\pi} \{ & e^{-j k_l r_0 \cos(\theta_{mn} - \alpha_0)} - e^{-j k_l r_1 \cos(\theta_{mn} - \alpha_1)} \\ & - e^{-j k_l r_2 \cos(\theta_{mn} - \alpha_2)} + e^{-j k_l r_3 \cos(\theta_{mn} - \alpha_3)} \}, \quad l = 1, 2, 3, \ldots, \end{aligned} \tag{A3}$$

where k_l, $l = 1, 2, 3, \ldots$ are the mean values of k_{mn} in each ring-shaped band. Accordingly, $w(x, y, k)$ is obtained by summing $w_{\Delta k}(k_l)$ over k_l:

$$w(x, y, k) = \sum_{k_l} w_{\Delta k}(k_l), \quad l = 0, 1, 2, 3, \ldots \tag{A4}$$

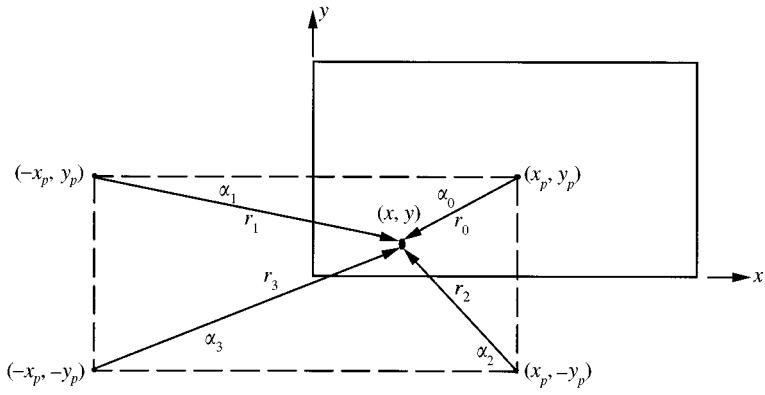

Figure A1. Geometry for r_i and α_i, $i = 0, 1, 2, 3$.

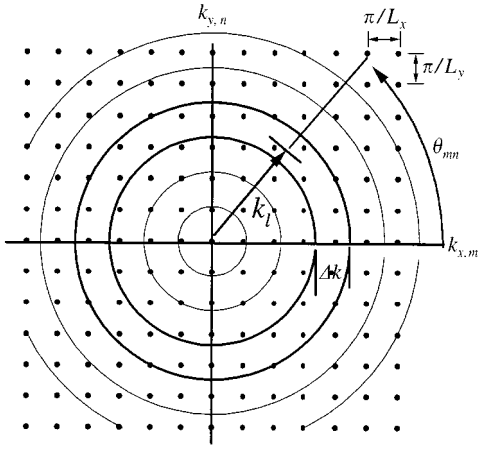

Figure A2. Mode lattice for a rectangular plate.

By assuming that the number of modes $N_{\Delta k}(k_l)$, $l = 1, 2, 3$, in each ring-shaped band is sufficiently large such that the angular interval $\Delta\theta_{mn}$ between two modes is small on average, the summation in equation (A3) can be approximated by an integral [3, 4], leading to

$$w_{\Delta k}(k_l) \approx \frac{F/4DA}{\Delta\theta_{mn}(k_l^4 - k^4)} \int_0^{2\pi} [e^{-jk_l r_0 \cos(\theta - \alpha_0)} - e^{-jk_l r_1 \cos(\theta - \alpha_1)}$$

$$- e^{-jk_l r_2 \cos(\theta - \alpha_2)} + e^{-jk_l r_3 \cos(\theta - \alpha_3)}] \, d\theta$$

$$= \frac{\pi F}{2DA} \frac{1}{\Delta\theta_{mn}} \frac{[J_0(k_l r_0) - J_0(k_l r_1) - J_0(k_l r_2) + J_0(k_l r_3)]}{k_1^4 - k^4}$$

$$= \frac{\pi F}{2DA\Delta\theta_{mn}} \frac{Q(k_l)}{k_l^4 - k^4}. \tag{A5}$$

Upon substituting equation (A5) into equation (A4),

$$w(x, y, k) \approx \frac{\pi F}{2DA} \sum_{l=0}^{\infty} \frac{1}{\Delta\theta_{mn}} \frac{Q(k_l)}{k_l^4 - k^4} \quad \text{for } x \leqslant x_p,\ y \leqslant y_p. \tag{A6}$$

From the lattice in Figure A2 the number of modes $N_{\Delta k}(k_l)$ in the band Δk is found to be

$$N_{\Delta k}(k_l) = \frac{2\pi k_l \Delta k}{(\pi/L_x)(\pi/L_y)} = k_l \frac{2A\Delta k}{\pi}. \tag{A7}$$

The averaged angular interval $\Delta\theta_{mn}$ is thus obtained as

$$\Delta\theta_{mn} = \frac{2\pi}{N_{\Delta k}(k_n)} = \frac{1}{k_l A} \frac{\pi^2}{\Delta k} \tag{A8}$$

Substituting equation (A8) into (A6) yields

$$w(x, y, k) \approx \frac{F}{D} \frac{\Delta k}{2\pi} \sum_{l=0}^{\infty} \frac{k_l}{k_l^4 - k^4} Q(k_l) \quad \text{for } x \leqslant x_p,\ y \leqslant y_p. \tag{A9}$$

Making use of the relations $2\mathrm{J}_0(z) = \mathrm{H}_0^{(2)}(z) + \mathrm{H}_0^{(1)}(z)$, $\mathrm{H}_0^{(2)}(z\mathrm{e}^{-\mathrm{i}\pi}) = -\mathrm{H}_0^{(1)}(z)$ [18] and evaluating the infinite series by using a contour integral [7–9] gives

$$\sum_{l=-\infty}^{\infty} \frac{k_l \mathrm{H}_0^{(2)}(k_l r_i)}{k_l^4 - k^4} = -\frac{\pi[\mathrm{H}_0^{(2)}(kr_i) - \mathrm{H}_0^{(2)}(-\mathrm{j}kr_i)]}{4k^2 \Delta k \tan(k\pi/\Delta k)}, \quad i = 0, 1, 2, 3 \tag{A10}$$

as is detailed in Appendix B. Accordingly,

$$w(x, y, k) \approx -\frac{F(S_0 + S_1 + S_2 + S_3)}{2\pi D k^2 \tan(k\pi/\Delta k)} \quad \text{for } x \leqslant x_p,\ y \leqslant y_p \tag{A11}$$

where

$$S_0 = +[\mathrm{H}_0^{(2)}(kr_0) - \mathrm{H}_0^{(2)}(-\mathrm{j}kr_0)] \qquad S_1 = -[\mathrm{H}_0^{(2)}(kr_1) - \mathrm{H}_0^{(2)}(-\mathrm{j}kr_1)]$$

$$S_2 = -[\mathrm{H}_0^{(2)}(kr_2) - \mathrm{H}_0^{(2)}(-\mathrm{j}kr_2)] \qquad S_3 = +[\mathrm{H}_0^{(2)}(kr_3) - \mathrm{H}_0^{(2)}(-\mathrm{j}kr_3)] \tag{A12}$$

APPENDIX B: EVALUATION OF AN INFINITE SERIES BY A CONTOUR INTEGRAL

Consider the sum

$$S = \sum_{n=-\infty}^{\infty} \frac{k_n \mathrm{H}_0^{(2)}(k_n r)}{k_n^4 - k^4}. \tag{B1}$$

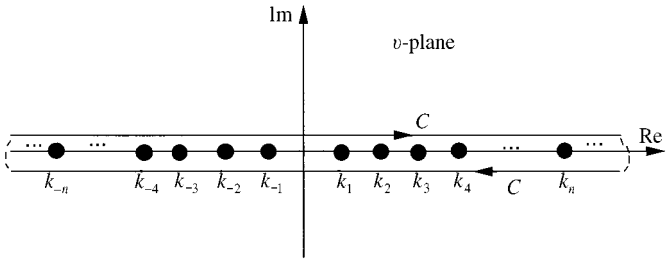

Figure B1. Integral contour C around real axis in v-plane.

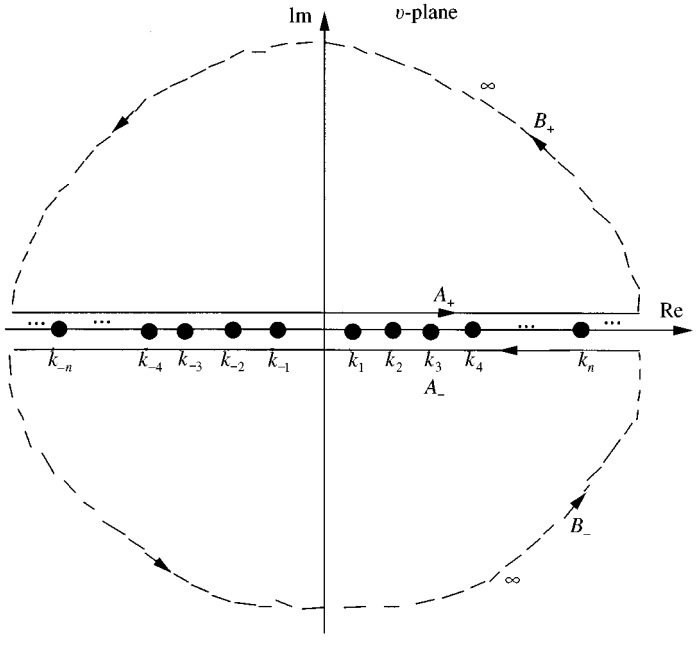

Figure B2. Contour C_+ consisting of A_+ and B_+, and the Contour C_- consisting of A_- and B_-

Upon allowing for k to be complex, the summation S can be expressed as a contour integral as [7–9]

$$\sum_{n=-\infty}^{\infty} \frac{k_n \mathrm{H}_0^{(2)}(k_n r)}{k_n^4 - k^4} = \frac{\mathrm{j}}{2} \oint_C \frac{\cos(\pi v) k_v \mathrm{H}_0^{(2)}(k_v r)}{\sin(v\pi)(k_v^4 - k^4)} \mathrm{d}v \tag{B2}$$

where C is the clockwise contour shown in Figure B1.

To proceed, the contour C is transformed into a contour C', which contains only the poles of $(k_v^4 - k^4)$ [7]. For this purpose, a contour C_+ is formed in the upper half-plane, and a similar contour C_- in the lower plane. Each contour consists of a semicircle of infinite radius B_+ or B_- at infinity, and a line parallel to the real axis A_+ or A_-, as shown in Figure B2.

The contour integrals are given by the residues at the poles of $k_v H_0^{(2)}(k_v r)/(k_v^4 - k^4)$ in the upper and lower half-plane, respectively, i.e.,

$$\oint_{C_+} = \int_{A_+} + \int_{B_+} = 2\pi \mathrm{j} \sum_n \kappa_n^{upper}, \qquad \int_{C_-} = \int_{A_-} + \int_{B_-} = 2\pi \mathrm{j} \sum_n \kappa_n^{lower}. \quad \text{(B3, B4)}$$

Since the integrals along the semicircles B_+ and B_- vanish as the radius $|v|$ tends to infinity, a summation of the two contour integrals gives

$$\oint_{C_+} + \oint_{C_-} = \int_{A_+} + \int_{A_-} = \oint_C. \tag{B5}$$

This means that

$$\oint_C = 2\pi \mathrm{j} \left\{ \sum_m \kappa_m^{upper} + \sum_n \kappa_n^{lower} \right\}. \tag{B6}$$

The zeros of $(k_v^4 - k^4)$ are found by solving for v the equation

$$(v\Delta k)^4 - k^4 = 0, \tag{B7}$$

which gives

$$v_1 = k/\Delta k, \quad v_2 = \mathrm{j}\, k/\Delta k, \quad v_3 = -k/\Delta k, \quad v_4 = -\mathrm{j}\, k/\Delta k. \tag{B8}$$

The poles v_2 and v_3 can be neglected because they make the point (x_p, y_p) a sink. Thus, the residues at the pole v_1 and v_4 are

$$\kappa_1 = \left. \frac{\cos(v\pi) k_v H_0^{(2)}(k_v r)}{\sin(k_v \pi)} \frac{1}{\mathrm{d}(k_v^4 - k^4)/\mathrm{d}v} \right|_{v = v_1} = \frac{1}{\tan(k\pi/\Delta k)} \frac{H_0^{(2)}(kr)}{4k^2 \Delta k}, \tag{B9}$$

$$\kappa_4 = \left. \frac{\cos(v\pi) k_v H_0^{(2)}(k_v r)}{\sin(k_v \pi)} \frac{1}{\mathrm{d}(k_v^4 - k^4)/\mathrm{d}v} \right|_{v = v_4} = \frac{1}{\tan(\mathrm{j}k\pi/\Delta k)} \frac{H_0^{(2)}(-\mathrm{j}kr)}{4k^2 \Delta k}. \tag{B10}$$

Therefore,

$$\oint_C \frac{\cos(\pi v) k_v H_0^{(2)}(k_v r)}{\sin(v\pi)(k_v^4 - k^4)} \mathrm{d}v = 2\pi \mathrm{j} \sum_n \kappa_n$$

$$= \mathrm{j} \frac{\pi}{2k^2 \Delta k \tan(k\pi/\Delta k)} \left\{ H_0^{(2)}(kr) + \frac{\tan(k\pi/\Delta k)}{\tan(\mathrm{j}k\pi/\Delta k)} H_0^{(2)}(-\mathrm{j}kr) \right\} \tag{B11}$$

Because of $k/\Delta k \gg 1$, when the damping is not small, the following approximations hold:

$$\tan(k\pi/\Delta k) \approx 1, \qquad \tan(\mathrm{j}k\pi/\Delta k) \approx -1, \tag{B12}$$

and equation (B11) is simplified to

$$\oint_C \frac{\cos(\pi v) k_v \mathrm{H}_0^{(2)}(k_v r)}{\sin(v\pi)(k_v^4 - k^4)} \mathrm{d}v = \mathrm{j} \frac{\pi\{\mathrm{H}_0^{(2)}(kr) - \mathrm{H}_0^{(2)}(-\mathrm{j}kr)\}}{2k^2 \Delta k \tan(k\pi/\Delta k)} \tag{B13}$$

Therefore, the sum asymptotically approaches

$$\sum_{n=-\infty}^{\infty} \frac{\mathrm{H}_0^{(2)}(k_n r_i)}{k_n^4 - k^4} = \frac{\mathrm{j}}{2} \oint_C \frac{\cos(\pi v) k_v \mathrm{H}_0^{(2)}(k_v r_i)}{\sin(v\pi)(k_v^4 - k^4)} \mathrm{d}v \tag{B14}$$

$$= -\frac{\pi\{\mathrm{H}_0^{(2)}(kr_i) - \mathrm{H}_0^{(2)}(-\mathrm{j}kr_i)\}}{4k^2 \Delta k \tan(k\pi/\Delta k)} \tag{B14}$$

APPENDIX C: NOMENCLATURE

$A = L_x L_y$	area of the plate
E	Young's modulus
G	shear modulus
$\mathrm{H}_0^{(2)}(z)$	zeroth order Hankel function of second kind
$\mathrm{j} = \sqrt{-1}$	
$\mathrm{J}_0(z)$	zeroth order Bessel function
$k_{m,x} = m\pi/L_x$	eigenvalue of beam function
$k_{n,y} = n\pi/L_y$	eigenvalue of beam function
$k_{mn} = \sqrt{k_{m,x}^2 + k_{n,y}^2}$	
k_l, $l = 1, 2, 3, \ldots$	mean of k_{mn} for the lth ring-shaped band
$k_L = \omega\sqrt{\rho/E}$	longitudinal wavenumber
$k_T = \omega\sqrt{\rho/G}$	shear wavenumber
k_f	flexural wavenumber
$k_{1,n}, k_{2,n}, k_{3,n}, k_{4,n}$	four types of wavenumber of cylindrical shells for the nth circumferential mode
L_x	side length
L_y	side length
$n(\omega)$	modal density
R	radius of cylindrical shells
$N_{\Delta k}(k_l)$	mode count over a ring-shaped band Δk
T_{qp}	motion transmissibility from point excitation at p to an arbitrary point q
$w_{\Delta k}(k_l)$	mode grouping over a ring-shaped band of radius k_l
Y_c	characteristic mobility
Y_{qp}	transfer mobility from point p to q
$\delta\omega$	average of angular frequency interval between two modes
$\Delta\omega = \eta\omega$	modal overlap bandwidth
$\Delta\theta_{mn}$	averaged angular interval of the modes over ring-shaped band
ρ	mass density
η	loss factor
$\varphi_m(x)$	eigenfunction
$\psi_n(y)$	eigenfunction
ω	angular frequency
ω_{ring}	angular ring frequency of the shell